NeuroImage 188 (2019) 92–101

Contents lists available at ScienceDirect

NeuroImage

journal homepage: www.elsevier.com/locate/neuroimage

Open-field PET: Simultaneous brain functional imaging and behavioural response measurements in freely moving small animals

Andre Z. Kyme [a,b,c,*,5], Georgios I. Angelis [b,c,5], John Eisenhuth [c], Roger R. Fulton [b,c,d], Victor Zhou [b,1], Genevra Hart [e,2], Kata Popovic [b,c], Mahmood Akhtar [b,c,3], William J. Ryder [b,c,4], Kelly J. Clemens [f], Bernard W. Balleine [e,2], Arvind Parmar [b,g], Giancarlo Pascali [b,g], Gary Perkins [g], Steven R. Meikle [b,c]

[a] Biomedical Engineering, School of Aerospace, Mechanical & Mechatronic Engineering, Faculty of Engineering and IT, The University of Sydney, Sydney, NSW, 2006, Australia
[b] Imaging Physics Laboratory, Brain and Mind Centre, The University of Sydney, Sydney, NSW, 2006, Australia
[c] Faculty of Health Sciences, The University of Sydney, Sydney, NSW, 2006, Australia
[d] Department of Medical Physics, Westmead Hospital, Sydney, NSW, 2145, Australia
[e] Brain and Mind Centre, The University of Sydney, Sydney, NSW, 2006, Australia
[f] School of Psychology, University of New South Wales, Sydney, NSW, 2052, Australia
[g] Australian Nuclear Science and Technology Organisation, Sydney, NSW, 2234, Australia

ARTICLE INFO

Keywords:
Awake animal PET
Behaviour
Kinetic modelling
Motion correction
Dopamine D2 receptors
Drug challenge

ABSTRACT

A comprehensive understanding of how the brain responds to a changing environment requires techniques capable of recording functional outputs at the whole-brain level in response to external stimuli. Positron emission tomography (PET) is an exquisitely sensitive technique for imaging brain function but the need for anaesthesia to avoid motion artefacts precludes concurrent behavioural response studies. Here, we report a technique that combines motion-compensated PET with a robotically-controlled animal enclosure to enable simultaneous brain imaging and behavioural recordings in unrestrained small animals. The technique was used to measure in vivo displacement of [^{11}C]raclopride from dopamine D2 receptors (D2R) concurrently with changes in the behaviour of awake, freely moving rats following administration of unlabelled raclopride or amphetamine. The timing and magnitude of [^{11}C]raclopride displacement from D2R were reliably estimated and, in the case of amphetamine, these changes coincided with a marked increase in stereotyped behaviours and hyper-locomotion. The technique, therefore, allows simultaneous measurement of changes in brain function and behavioural responses to external stimuli in conscious unrestrained animals, giving rise to important applications in behavioural neuroscience.

1. Introduction

Interactions between an animal and its environment are complex. How these interactions are encoded in the brain and used to guide future behaviour is an area of intense study, exploiting a wide range of microscopic and macroscopic measurement techniques such as patch clamp recordings and 2-photon imaging (Chen et al., 2013). For the most part, these techniques are performed with the animal under anaesthesia and/or rigidly fixed in a stereotactic frame. More recently, several of these methods have been extended to enable localised recordings in awake, freely moving animals following surgical implantation or attachment of the requisite probe (Belle et al., 2013; Helmchen et al., 2001; Vyazovskiy et al., 2011). However, these methods are invasive, prone to imprecise sampling of the neuronal population of interest and

* Corresponding author. Biomedical Engineering, School of AMME, Faculty of Engineering & IT, The University of Sydney, Darlington, NSW, 2006, Australia.
E-mail address: andre.kyme@sydney.edu.au (A.Z. Kyme).
[5] Joint first authors.
[1] Now with Central Queensland University, Mackay, QLD 4740, Australia.
[2] Now with the Decision Neuroscience Laboratory, School of Psychology, University of New South Wales, Sydney, NSW 2052, Australia.
[3] Now with the Faculty of Engineering, University of New South Wales, Sydney, NSW 2052, Australia.
[4] Now with the Health Education and Training Institute, Royal Prince Alfred Hospital, Sydney, NSW 2050, Australia.

https://doi.org/10.1016/j.neuroimage.2018.11.051
Received 24 May 2018; Received in revised form 1 November 2018; Accepted 27 November 2018
Available online 28 November 2018

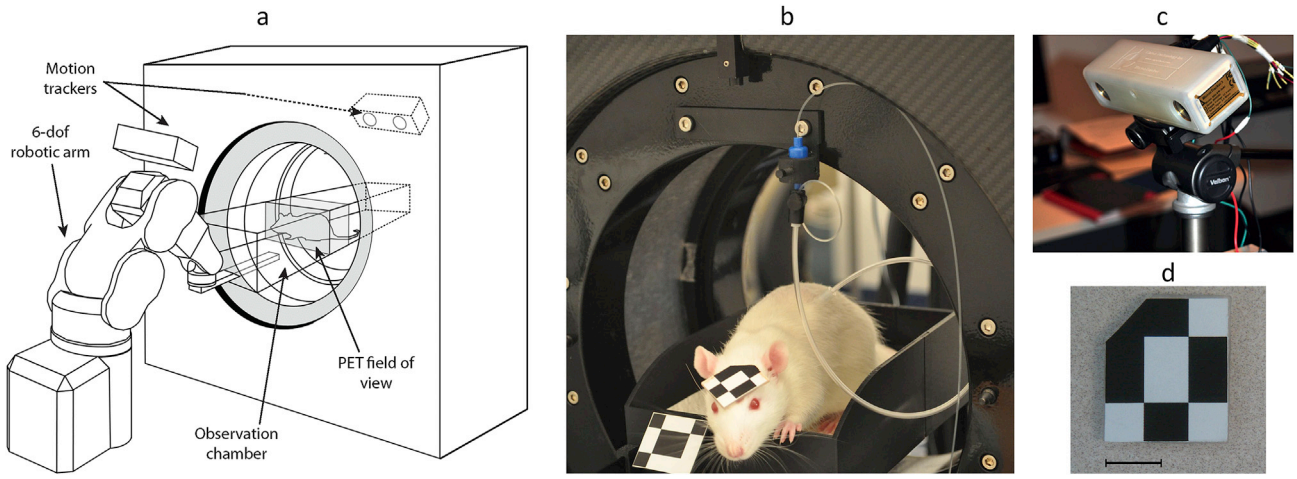

Fig. 1. Open-field PET experimental setup
(a) The experimental setup for the open-field PET technique, consisting of an unmodified small animal PET system, a robot-controlled animal enclosure and optical motion tracking devices at the front and rear of the PET gantry; (b) the catheterised, freely moving animal connected to a syringe pump (not visible in this figure) via a swivelled injection line; (c) the motion tracking system which uses a pair of CCD cameras to determine the rigid-body motion of three printed markers, one small lightweight marker attached to the animal's forehead (b and d, scale bar = 1 cm), another marker attached to the enclosure, and a third marker attached to the PET scanner (not visible in this figure).

confined to small pre-determined anatomical regions of the brain. A more complete understanding of how the brain responds to a changing environment requires new techniques capable of recording functional outputs at the whole-brain level in response to external stimuli, while retaining cell and receptor type specificity.

High resolution small animal positron emission tomography (PET) has the potential to advance our understanding of the signalling pathways involved in cognition and behaviour under normal and pathological conditions. With the appropriate choice of positron-emitting radiopharmaceutical, PET provides a quantitative 3D map of blood flow, metabolism or receptor-ligand binding throughout the rodent brain, including animal models of disease (Chatziioannou, 2002), with pico-molar sensitivity. Importantly, since PET is a non-invasive, non-terminal procedure, it also enables the longitudinal study of these processes during normal development and disease progression, including responses to therapeutic intervention or environmental stressors. Conventional PET technology requires the animal to remain motionless throughout the 1- to 2-h scanning procedure, typically achieved by anaesthesia and rigid fixation of the head. However, the routine use of anaesthesia not only perturbs many of the neurological parameters of interest, such as blood flow, neural-hemodynamic coupling and receptor binding (Nakao et al., 2001; Tantawy et al., 2011), it also precludes the use of functional imaging to relate changes in neurotransmitter activity and receptor binding to behavioural adaptation in response to environmental cues or drug administration (Cherry, 2011).

Several approaches have been developed in an attempt to mitigate the confounding effects of anaesthesia, although limitations with all of these methods have restricted their utility. For example, one approach is to inject the PET tracer, then to present the desired stimulus while the animal is conscious, and later to anaesthetise the animal for imaging (Thanos, 2013). This approach is mainly limited to PET tracers that are irreversibly trapped in the cell, such as 2-deoxy-2-[^{18}F]fluoro-D-glucose (FDG), thus allowing a delayed 'snapshot' image of brain function that reflects the peri-stimulus state. While similar methods have been used in conjunction with reversible receptor-binding PET ligands (Patel et al., 2008; Tantawy et al., 2011), they do not enable real-time measurement of transient changes in receptor binding at the onset of the stimulus. Another approach is to rigidly attach a miniature PET detector ring to the head of the animal (Vaska et al., 2004; Shulz et al., 2011). Although this method enables dynamic imaging of awake rats with receptor-binding PET ligands, together with a limited range of behavioural assays, it requires invasive surgery to attach the imaging apparatus to the head and the inertia of the attached detector ring restricts natural movement of the animal. Finally, the feasibility of tethering the skull of a mouse to a rigid head fixation device while undergoing PET imaging in the conscious state has been demonstrated (Mizuma et al., 2010). However, this technique requires extensive training and acclimatisation, provides for only a limited variety of behavioural response assays, and is subject to the confound of stress-induced physiological changes.

To overcome these limitations, we developed an open-field PET imaging technique that enables the brain of an unrestrained rat to be imaged in an unmodified small animal PET scanner, while simultaneously recording behavioural outputs following the delivery of controlled stimuli. The technique combines advanced motion estimation and motion-compensated image reconstruction methods, a robotically-controlled animal enclosure conducive to behavioural testing, and a tracer/drug delivery protocol that accommodates a freely moving animal. Here we describe the open-field PET system and associated methodology and demonstrate the simultaneous measurement of changes in regional D2 receptor (D2R) binding and behavioural responses to pharmacological stimuli in conscious, unrestrained rats.

2. Methods

2.1. Open-field PET system overview

The open-field PET system comprises a commercial PET scanner, optical motion tracking and a custom designed motion-adaptive animal enclosure attached to a 6-axis robotic arm (Fig. 1a). Motion tracking (Fig. 1a, c) from both ends of the PET gantry enables measurement of the changing position and orientation of a small lightweight marker attached to the forehead of the animal (Fig. 1b, d). Reconstruction of quantitatively accurate, motion-corrected PET images requires accurate calibration and synchronisation of head pose estimates with data acquired by the PET scanner (Kyme et al. 2008, 2012) and an event-by-event (list mode) motion-corrected image reconstruction algorithm (Rahmim et al., 2008; Zhou et al., 2008).

2.1.1. PET scanner

The open-field PET system is built around the microPET Focus 220 preclinical PET scanner (Preclinical Solutions, Siemens Healthcare Molecular Imaging, Knoxville, TN, USA), which comprises lutetium

oxyorthosilicate (LSO) scintillation detectors coupled to photomultiplier tubes. The Focus has a bore diameter of 220 mm, a transaxial field of view (FoV) of 190 mm and an axial FoV of 76 mm. Spatial resolution and coincidence photon detection sensitivity at the centre of the FoV are 1.3 mm FWHM and 3.4%, respectively (Tai et al., 2005). All data were recorded in list mode (event-by-event) format and stored locally for offline processing.

2.1.2. Motion tracking

Two MicronTracker Sx60 binocular tracking systems (ClaroNav, Toronto, Canada) were located at opposite ends of the scanner bore (Fig. 1a) to track the rigid-body pose (position and orientation) of the animal's head and the enclosure with 0.2 mm RMS positional accuracy. Both trackers were oriented at 45° declination and positioned 0.5 m from the centre of the scanner FoV in accordance with the optimised geometry described in Kyme et al. (2012). The two trackers were spatially calibrated to a common reference frame in which all marker measurements were reported, regardless of which tracker detected the marker. The tracking frame was also cross-calibrated to the PET scanner frame so that PET lines-of-response could be motion-corrected offline.

Three separate markers were tracked during our experiments: a marker attached to the animal's head (Fig. 1b, d), a marker attached to the moving enclosure (Fig. 1b), and a reference marker permanently fixed to the PET gantry. The reference marker enabled convenient updating of the tracker-scanner cross-calibration in each new experiment without having to repeat the cross-calibration procedure. Details of this approach are described in Kyme et al. (2011). The enclosure marker comprised two large L-shaped facets, one at each end of the enclosure. Position measurements of the enclosure were fed to the robot controller software (section 2.1.4) in real time to prevent collisions between the enclosure and gantry as the position of the enclosure was adjusted in response to animal motion. The head marker comprised a single L-shaped facet on a 3D-printed substrate (Fig. 1d), which was affixed to a small shaved patch on the animal's forehead (Fig. 1b) using a drop of cyanoacrylate (super glue). Using this approach, markers remained firmly attached to the scalp for several hours.

During an experiment, the changing pose of each marker was measured at 30 Hz. The (x, y, z) position of the head marker was transformed to the PET coordinate frame in real time and input to the robot controller software for adaptive enclosure position control in response to animal motion. The full pose (i.e. position and orientation component) of the head marker was stored for offline motion compensation of the PET data. Triggering of the front- and rear-side trackers occurred simultaneously using a square-wave generator (TTL, positive polarity, half-duty cycle, 30 Hz). Each trigger pulse initiated sensor exposure for each tracker and also triggered a square pulse (TTL, positive polarity, 15 ms duration) from the front-side tracker to the gating input on the PET scanner. Receipt of this pulse at the scanner gating input resulted in the insertion of a gating 'tag-word' in the PET event data stream. Matching of these tag-words with the triggered pose measurements allowed us to synchronise the two data streams for motion compensation. To enable rapid (5 ms) exposure of the CCD cameras in the tracking systems, we bounced the light from two 1000-W halogen work lights off the ceiling to give a diffuse illuminance of approximately 450 Lux inside the scanner FoV. The lights were positioned symmetrically on either side of the scanner, out of direct sight of the animals.

2.1.3. Animal enclosure

The motion-adaptive animal enclosure is a structurally rigid, lightweight and minimally attenuating box consisting of multiple 3D-printed interlocking sections of acrylonitrile butadiene styrene (ABS) thermoplastic supported by carbon fibre ribs which run the length of the enclosure to thread the sections together for additional stability and to resist flexing about the longitudinal axis. The enclosure is 120 mm wide and adjustable in length from 200 to 500 mm. All of our experiments were performed using a length of 220 mm. The enclosure is designed with an optional computer-interfaced lever press and reward delivery mechanism. This allows the enclosure to be used either as a simple observation chamber for studying animal behaviour, or as an operant chamber for instrumental conditioning experiments. A 3D-printed adaptor was used to secure the enclosure to the robot end-effector.

2.1.4. Robot positioning and control

The 6-axis robot (Epson C3-A601S, Seiko Corp., Japan) used to adaptively position the animal enclosure in response to animal motion was mounted to a custom-built trolley adjacent to the PET gantry. The robot was programmed to translate the enclosure in response to measured head movements. These translations were sufficiently slow and smooth to avoid startling the animal. The basic motion control algorithm for compensatory enclosure positioning is described in detail in Zhou et al. (2013). However, rather than perform compensatory movements of the enclosure using the sector-based method described previously, we adapted the algorithm to translate the enclosure along the exact straight-line trajectory from its current position to the centre of the scanner FoV. In addition, whenever the head marker was obstructed from both trackers (i.e. no updated head position information was available), the robot would automatically return the marker to the centre of the scanner FoV based on its last known position. This 'recovery mode' was intended to rapidly restore tracking and, thereby, maintain close to uninterrupted robotic compensatory motion.

2.1.5. Motion compensation and image reconstruction

All reconstructions were performed using 10 iterations and 10 subsets of an iterative ordered subsets expectation maximisation (OSEM) list mode reconstruction algorithm incorporating motion compensation according to the method described in Rahmim et al. (2008). The acquired list-mode events were pre-corrected for motion on an event-by-event basis using the pose information obtained from the motion tracker (Zhou et al., 2008). Corrections for normalisation were included within a motion-dependent, time-weighted sensitivity image (Rahmim et al., 2008), while events were corrected for photon attenuation using a transmission-less calculated attenuation correction approach (Angelis et al. 2013, 2014). Scatter correction was not performed since the scatter fraction is <15% for the rat brain. We also applied a shift-invariant resolution model during the reconstruction based on an empirically defined resolution kernel corresponding to the scanner resolution at the centre of the FoV.

2.2. Animal management

2.2.1. Animals

Male wild-type Sprague-Dawley rats were used for the imaging experiments. The animals were healthy, pathogen-free, drug naïve and had not been used in previous experimental procedures. For the reproducibility study (section 3.1), four 10-week old animals (mean weight 304 ± 26 g, range 256–330 g) were scanned on two consecutive days. For the simultaneous open-field PET and behavioural response study (section 3.2), three 15-week old animals (mean weight 442 ± 17.6 g, range 421–465 g) were scanned on two consecutive days. Animals were group-housed in ventilated cages and maintained on a 12-h:12-h light:dark cycle with food and water *ad libitum*. All animal management and experimentation was performed in accordance with protocols approved by the University of Sydney Animal Ethics Committee and consistent with National Institutes of Health guidelines.

2.2.2. Surgery

One week after arrival rats were implanted with a chronic indwelling catheter in the right jugular vein. Rats were anaesthetised with 2–3% inhalation isofluorane in oxygen (2 L/min) and injected with a pre-emptive analgesic (Carprofen, 5 mg/kg s.c.). A custom-made catheter consisting of silastic tubing (internal diameter (ID) 0.5 mm, outer diameter (OD) 1.5 mm, Dow Corning) was inserted 25 mm into the

jugular vein, terminating in the heart. The distal end passed subcutaneously to exit posterior to the scapulae and terminated with a 22-gauge back mount cannula (Plastics One, USA). The back mount was secured in place with a suture and flushed daily with cephazolin sodium antibiotic (0.2 mL, 100 mg/mL) in sterile saline (0.9%). Following three days of recovery, heparin (150 I.U/mL) was added to the antibiotic solution to minimise catheter blockage. Catheters were flushed daily with heparinised cephazolin for the remainder of the first week and then every 2–3 days thereafter. Rats were allowed seven days to recover from surgery before commencing acclimatisation, training and imaging experiments.

2.2.3. Acclimatisation protocol

One week after surgery the rats were systematically acclimatised to the imaging environment and open-field apparatus over four days: day 1 was basic familiarisation with the scanner environment for 30 min without a head marker or tethered catheter; on days 2–4 the animals were habituated for 45 min to the full experimental conditions, including the attached head marker, tethered catheter and robotic motion compensation. The lighting (room lights and auxiliary lights) and positions of all stationary apparatus (video cameras, syringe pump, computers, motion tracking systems and cabling) required for imaging on days 5 and 6 were identical during the acclimatisation sessions to avoid introducing novel visual cues. Acclimatisation sessions were video recorded for each animal to monitor behavioural patterns. Posture, gait, respiration and activity for all animals were found to be normal.

2.3. Radiotracer and drug infusion

[^{11}C]Raclopride was synthesised according to Perkins et al. (2014). A 30 cm cannula connector made of flexible plastic tubing (ID 1.93 mm, OD 2.74 mm, Plastics One, USA) was used to connect the jugular port on the scapula to a stainless steel swivel (Instech Laboratories Inc., USA) fixed to the scanner gantry. Cannula tubing (ID 0.58 mm, OD 0.96 mm, Microtube Extrusions, Australia) was inserted through the connector for tracer and drug infusion. The thick connector tubing provided protection against the animal chewing through the infusion line. From the swivel, the cannula tubing connected to a syringe loaded in a syringe pump (Harvard Pico Plus, USA). Altogether, the length of cannula tubing from syringe to animal had a volume of 320 μL. This enabled us to safely load 250 μL of tracer in the infusion line prior to beginning a slow bolus infusion at the start of the imaging study. The tracer was infused over 38 s by pumping 600 μL of sterile saline (0.9%) through the line at 400 μL min^{-1}. This volume of saline completely flushed the line once the tracer volume was expelled. For drug infusion, 140 μL was loaded into the line and infused over 15 s by pumping 400 μL of sterile saline through the line at 400 μL min^{-1}. The total injected volume for each rat was 1.35 mL (~5% total blood volume). Raclopride was administered as unlabelled raclopride in 0.9% sterile saline (100 μL, 2 mg kg^{-1}). Amphetamine was administered as D-amphetamine dissolved in 0.9% sterile saline (100 μL, 2 mg kg^{-1}).

2.4. Data analysis

2.4.1. PET data analysis

Transient changes in physiology following drug administration have been shown to cause time-dependent fluctuations in radiotracer delivery and clearance (Alpert et al., 2003), thus conventional steady state models are invalid. Accordingly, decay-corrected PET time-activity curves were fitted with the linear parametric neurotransmitter PET (lp-ntPET) model (Normandin et al., 2012), which is a generalisation of the multi-linear reference tissue model (MRTM) (Ichise et al., 2003) that includes a time-varying term to describe the non-steady state condition. The lp-ntPET model leads to the following operational equation describing the tracer concentration in the target region-of-interest (ROI) (the striatum in our case), C_T, as a function of time, t:

Table 1
Categorisation of animal behaviours.

Behaviour	Description
Sleep	Asleep or immobile in resting position for greater than 30 s
Groom	Head or body grooming
Locomotion	Repetitive (>3 reps) gross movement of whole body or head and shoulders, e.g. rearing towards the top of the scanner then leaning towards the bottom
Head-up sniff	Head tilted upwards, sniffing in reared or non-reared position
Head-down sniff	Head tilted downwards, sniffing the bottom of the scanner or chamber
Mouth movements	Non-specific oral movements, tongue protrusions, air licking
Chew	Chewing the chamber flooring, walls etc.
Perch	Positioned with hind legs on or near the wall of the chamber, body balanced over the edge, front paws either in the air or on the wall of the chamber
Head bob	Fast upward and downward head movements

$$C_T(t) = R_1 C_R(t) + k_2 \int_0^t C_R(u)du - \int_0^t (k_{2\alpha} + \gamma h_i(u))C_T(u)du \quad (1)$$

where C_R is the tracer concentration in the reference ROI (cerebellum) and $\theta = [R_1, k_{2\alpha}, \gamma]$ are the model coefficients. R_1 is the delivery ratio and k_2 is the eflux rate from free compartment back to plasma. The transient perturbation of the system is modelled by $\gamma h_i(t)$ which represents the time course of the activation, with γ encoding the magnitude of the effect. As in Normandin et al. (2012), we modelled $h_i(t)$ as a series of gamma variate functions spanning a wide range of feasible shapes and possible times of onset (from 10 to 40 min at 1.5 min intervals). The lp-ntPET model was fitted to the PET data using a weighted least squares and basis pursuit strategy. The key model output from this fitting procedure in ligand displacement studies is the time-dependent tracer efflux from the compartment representing specifically bound tracer:

$$k_{2\alpha}(t) = k_{2\alpha} + \gamma h(t) \quad (2)$$

where $h(t)$ represents the gamma variate function that best fits the data and describes the activation effect.

Fitting the lp-ntPET model as described provides model parameter point estimates but does not tell us about the reliability of those estimates. To evaluate the reliability we used the Monte Carlo based Approximate Bayesian Computation (ABC) algorithm (Marin et al., 2012). This method involves conducting a very large number (~millions) of trials using model parameters drawn randomly from a prior distribution, in our case an uninformative uniform prior. For each trial, the model-based PET curve is estimated according to equation (1) and compared with the measured PET curve. The trial is either accepted or rejected based on the sum of squared differences between the two curves and a predetermined threshold. After many such trials, the model curves which are accepted have sufficient statistics to form a histogram of parameter estimates that provide an excellent approximation of the posterior probability density functions (PDF) of those parameters. As well as computing PDFs, we also calculated median and 95% confidence intervals for the $k_{2\alpha}(t)$ term from the sub-population of accepted model curves, i.e. the successful trials.

2.4.2. Motion data analysis

Locomotor activity response as a function of time was determined directly from the motion tracking data and reported in units of cm.s^{-1}.

2.4.3. Behavioural data analysis

In addition to the locomotor response, stereotyped and non-stereotyped behaviours exhibited by the rat during the open-field PET scans were analysed manually using a time sampling procedure adapted from Kelley (1998). The rat was observed every minute throughout each of the open-field PET scans and scored according to the presence or absence of each of nine behaviours, which are summarised in Table 1. A

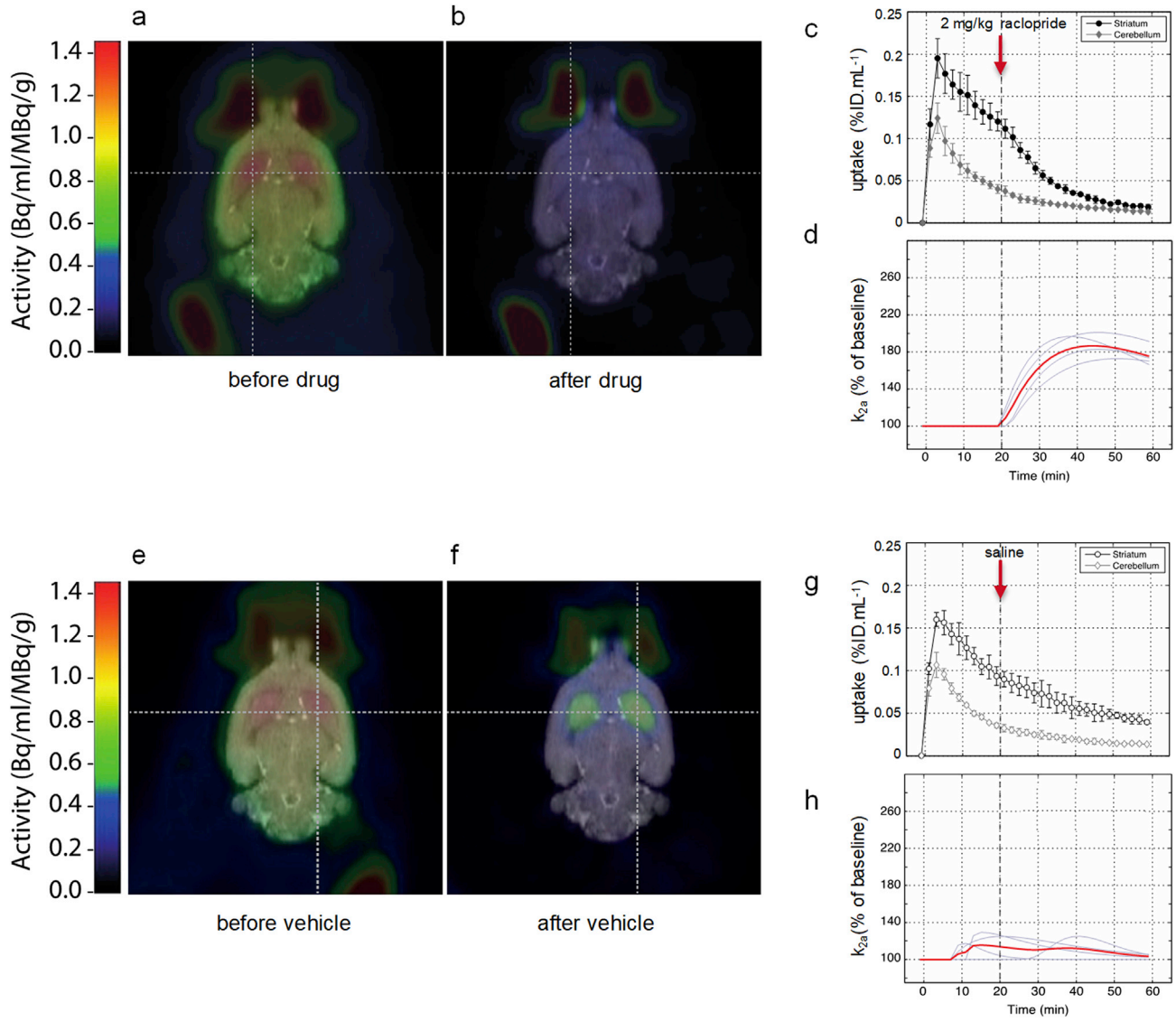

Fig. 2. Reproducibility of the open-field PET technique
(a) Motion-corrected PET data showing the integrated [^{11}C]raclopride distribution in the brain of a representative freely moving rat over the first 20 min of the study (prior to the administration of unlabelled raclopride), superimposed on a spatially registered MRI brain template; (b) reconstructed PET image integrated over the last 20 min of the study, after administration of unlabelled raclopride; (c) PET time-activity curves averaged across four animals (mean ± 1 s d) for striatal and cerebellar regions of interest; and (d) the four individual (grey) and mean (red) estimated D2R displacement ($k_{2\alpha}$) curves obtained from kinetic modelling of the dynamic PET data in (c). The images and graphs in panels e–h are the corresponding data obtained from the animals administered a saline vehicle 20 min into the PET study instead of unlabelled raclopride.

behavioural score was calculated as the proportion of time the rat engaged in each behaviour.

3. Experiments

3.1. Reproducibility of the open-field technique

We evaluated the ability of the open-field technique to reliably estimate changes in D2R binding in the brains of freely moving rats. Four adult male Sprague-Dawley rats were scanned on two consecutive days. For both scans the rats were administered [^{11}C]raclopride (mean 48 ± 18 MBq, 0.84 ± 0.16 nmol) via the indwelling jugular vein catheter and imaged in the open-field PET system for 60 min. For one PET scan, the animals were administered 2 mg kg^{-1} of unlabelled raclopride 20 min after tracer injection. Based on previous studies, this dose of raclopride is expected to occupy close to 100% of available D2 receptors in the rat brain and cause nearly complete displacement of the tracer from D2R binding sites (Hume et al. 1995, 1998). For the other PET scan, an identical protocol was used except that a saline vehicle was administered at 20 min instead of unlabelled raclopride. The order of the scans was counterbalanced across animals. From the reconstructed and decay-corrected dynamic frames we generated curves representing the regional temporal characterisation of the increased efflux rate (displacement) from the striatum.

3.2. Simultaneous open-field PET and behavioural response studies

The purpose of the previous experiment was to demonstrate that the open-field PET method can reliably estimate changes in dopamine receptor occupancy. To illustrate the use of the approach in combined behavioural and receptor-ligand imaging studies, we measured D2R displacement in the cold raclopride challenge and following administration of the psychostimulant drug, amphetamine. In addition to a nearly complete displacement of the radiotracer from the D2 receptors,

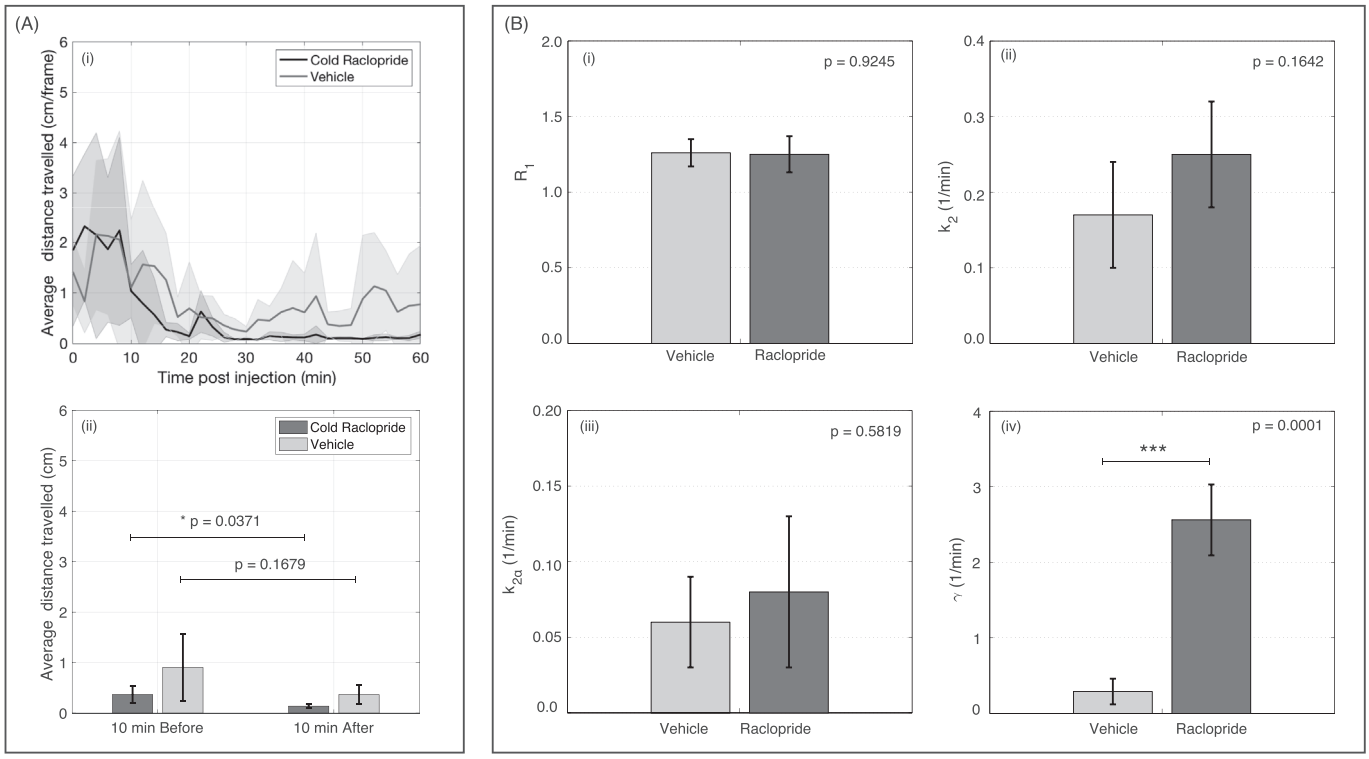

Fig. 3. Motion and kinetic model parameters for the cold raclopride challenge.
(A.i) Average distance travelled as a function of time (shaded areas correspond to ±1 standard deviation) for the cold raclopride/saline scans; (A.ii) average distance travelled over 10 min before and 10 min after the injection of cold raclopride/saline; (B) estimated kinetic model parameters averaged across 4 animals for the cold raclopride/saline injection experiments (asterisks indicate significance at the $p < 0.001$ level; paired *t*-test).

injection of a pharmacological dose of cold raclopride may also lead to reduced locomotor activity and avoidance behaviours (Hillegaart and Ahlenius, 1987). On the other hand, amphetamine stimulates endogenous dopamine release from synaptic vesicles causing indirect competition with [^{11}C]raclopride for post synaptic D2R binding sites. This intervention is also expected to result in robust behavioural changes, such as hyperactivity and stereotypy (Schiorring et al., 1979). For the amphetamine challenge, three adult male Sprague-Dawley rats underwent two open-field PET studies on consecutive days. For each scan, the animal was injected with [^{11}C]raclopride (mean 39 ± 15 MBq, 0.82 ± 0.35 nmol) via the indwelling jugular vein catheter and imaged in the open-field PET system for 60 min. For the first PET scan, the animal was administered 540 µl of a saline vehicle via the catheter 20 min after tracer injection. For the second PET scan, the same protocol was used except that 2 mg kg^{-1} of amphetamine was administered. Dynamic PET data were analysed by least squares fitting of striatal time-activity curves with the lp-ntPET model which estimates the magnitude and timing of tracer displacement from the receptor-ligand complex (Normandin et al., 2012). To assess the reliability of model estimates, the posterior probability density distributions of displacement parameters were further analysed using ABC (Marin et al., 2012). The velocity of the animal's head in the horizontal plane was calculated at 2-min intervals throughout the PET study. These data were used as a proxy for locomotor activity and compared with the timing and magnitude of [^{11}C]raclopride displacement. In addition, video data acquired throughout each PET study were analysed using a time sampling procedure adapted from Kelley (1998) to measure a variety of stereotypical and non-stereotypical behaviours.

During all open-field imaging experiments the rats were free to move around the enclosure and, since it had no roof, were also able to lean over the sides. The floor of the enclosure was covered in absorbent towels to collect excrement and radioactive urine safely. All experiments were filmed from the front of the scanner using a video camera positioned 0.7 m from the centre of the scanner FoV.

4. Results

4.1. Reproducibility of the open-field PET technique

Motion-corrected images integrated over the 20 min immediately prior to drug/saline injection and for the last 20 min of the scan are shown for the drug and saline vehicle scans of one representative rat in Fig. 2a,b and 2, respectively. Decay-corrected striatal and cerebellar tracer uptake curves averaged across all four animals, after normalising for injected dose and body weight, are shown in Fig. 2c and g for the drug and vehicle scans, respectively.

The dynamic data were analysed by least squares fitting of individual striatal time-activity curves with the lp-ntPET ligand displacement model using the corresponding cerebellar curve as the input function (see Section 2.4.1). The model-estimated ligand displacement curves $k_{2\alpha}(t)$ for the drug challenge and vehicle-only scans are shown in Fig. 2d and h, respectively. The time-activity curves and displacement curves demonstrate a high degree of inter-subject reproducibility. Estimated time of onset of the displacement caused by injection of unlabelled raclopride, averaged across the four animals, was $t_d = 19.5 \pm 1.2$ min, which agrees well with the time of drug administration, and the peak amplitude of displacement was 1.85 ± 0.2 x baseline. The small magnitude, temporally misaligned false positive displacements seen in the null condition (Fig. 2h) are typical features of the lp-ntPET method when applied to noisy PET data (Normandin et al., 2012).

4.2. Simultaneous open-field PET and behavioural response

4.2.1. Cold raclopride

Fig. 3A i shows locomotor activity averaged across the 4 subjects (the shaded areas correspond to the ±1 standard deviation envelope) binned into 2-min frames (i.e. equal to the duration of the functional frames) for both the saline-vehicle and cold raclopride injections. To quantitatively

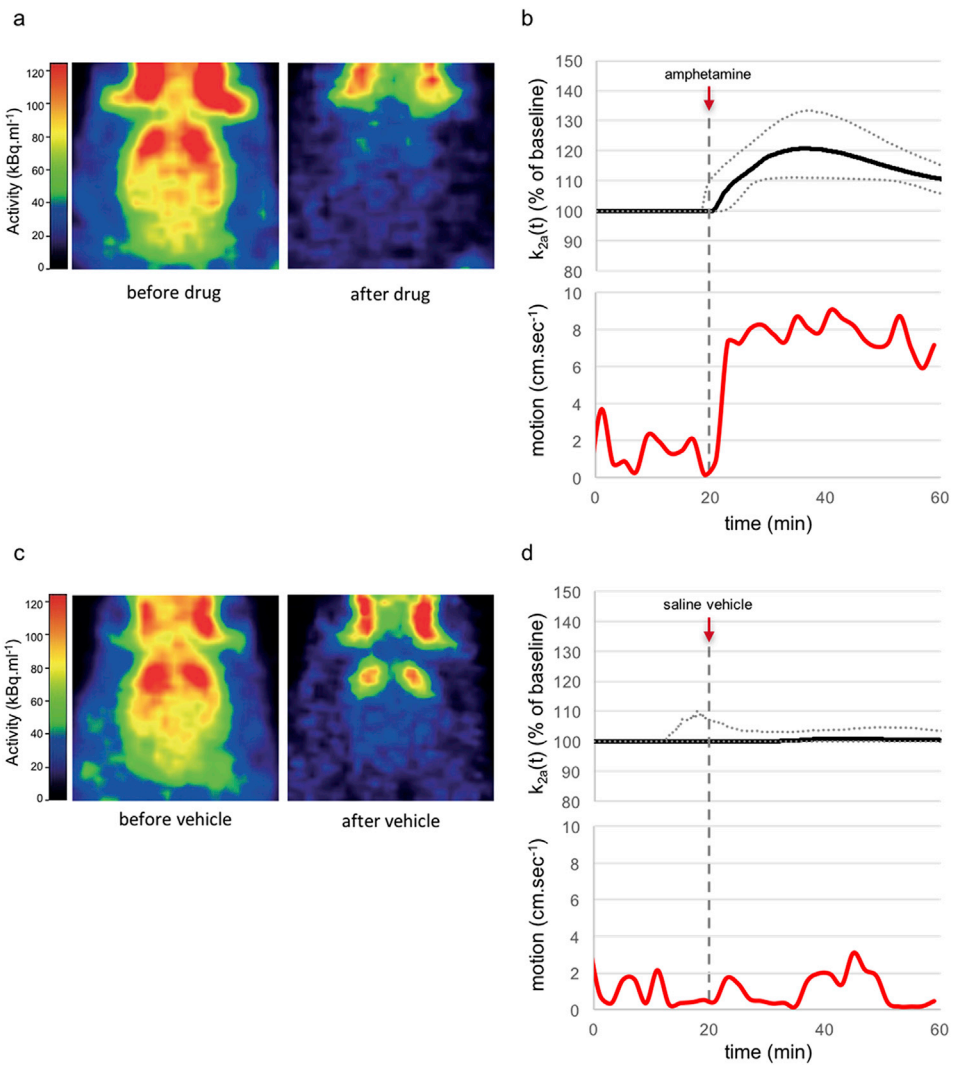

Fig. 4. Simultaneous open-field PET and behavioural response to amphetamine challenge

(a) Motion-corrected PET images (co-registered to a MRI brain template) showing the integrated [^{11}C]raclopride distribution in the brain of a representative freely moving rat integrated over the 20 min prior to drug administration (left) and over the last 20 min of the study (right); (b) estimated D2R displacement ($k_{2\alpha}$) curves (±95% CI) for the striatum (upper) and the locomotor activity throughout the PET study (lower) for the animal receiving amphetamine. Panels c and d show the corresponding tracer distributions, D2R displacement curve and motion data when the same animal underwent a separate PET scan and received only the saline vehicle 20 min after [^{11}C]raclopride injection.

assess the change in behaviour before and after injection of the drug or vehicle, we averaged the distance travelled by the animals 10 min before injection and 10 min after (Fig. 3A ii). There was a slight reduction in locomotor activity after injection of cold raclopride which reached statistical significance ($p < 0.05$), whereas saline had no significant effect on behaviour ($p = 0.1679$). We believe that the behavioural effect of raclopride did not reach a greater level of significance due to the 'floor effect', where the animals were already exhibiting relatively low levels of motor activity prior to injection. Fig. 3B shows the group-average parameter estimates of the lp-ntPET model, highlighting a significant change in the non-steady state parameter γ describing the magnitude of activation (i.e. increased efflux rate) after drug administration, and insignificant differences for the steady-state parameters, R_1, k_2 and $k_{2\alpha}$.

4.2.2. *Amphetamine*

Fig. 4a shows the motion-corrected [^{11}C]raclopride distribution in the brain integrated over the first 20 min of the study (left panel), i.e. prior to amphetamine administration, and over the last 20 min of the study (right panel), i.e. after amphetamine administration, for a representative subject. An appreciable displacement of the specific D2R binding signal in the striatum is seen in the post drug administration image. The lp-ntPET model output curve (Fig. 4b, upper panel) also indicates a clear displacement of the tracer from D2R binding sites whose time of onset is consistent with the time of drug administration and which reaches a peak amplitude of 120% of baseline 15–20 min after drug administration. The displacement also correlated with a pronounced increase in head motion (average post-drug motion = 543% of average pre-drug motion) that was sustained until the end of the imaging study (Fig. 4b, lower panel). There was no change in specific D2R binding in the striatum observed on either the integrated PET images (Fig. 4c) or displacement curves (Fig. 4d, upper panel) in the saline vehicle scan. The differences between the pre- and post-vehicle images, including extra-striatal regions, can be explained by changes in blood flow (which are accounted for by the lp-ntPET model) and normal biological clearance. Similarly, there was no observable change in behaviour following vehicle administration (Fig. 4d, lower panel).

Fig. 5A i shows the average locomotor activity across the 3 animals. In contrast to the cold raclopride study, amphetamine produced a clear and sustained increase in locomotor activity shortly after injection of the drug, which was consistent across the 3 animals. Similar to the cold raclopride analysis, we averaged the distance travelled by the animals 10 min before and 10 min after the injection of the drug (Fig. 5A ii). The injection of amphetamine led to a behavioural effect that was highly significant ($p < 0.001$; paired *t*-test), whereas saline caused no significant effect ($p = 0.4125$). The change in behaviour due to the injection of amphetamine was also clearly evident by visually observing the animal (Fig. 6). We also averaged the estimated kinetic model parameters across the 3 animals (Fig. 5B) which shows a highly significant ($p < 0.005$; paired *t*-test) increase in activation magnitude, γ, for amphetamine compared with vehicle-only scans, and small but insignificant decreases

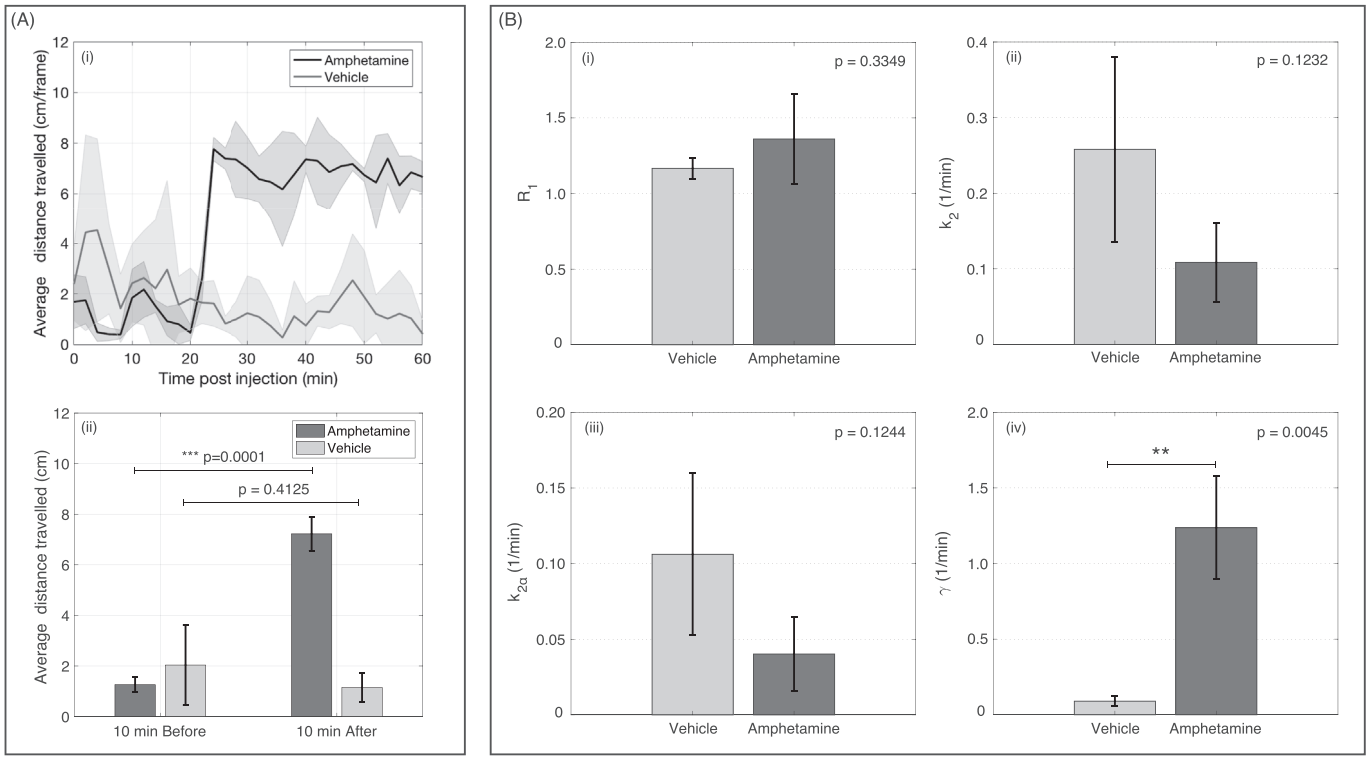

Fig. 5. Motion and kinetic model parameters for the amphetamine challenge.
(A.i) Average distance travelled as a function of time (shaded areas correspond to ±1 standard deviation) for the amphetamine/saline scans; (A.ii) average distance travelled over 10 min before and 10 min after the injection of amphetamine/saline (asterisks indicate significance at the $p < 0.001$ level; paired *t*-test); (B) estimated kinetic model parameters averaged across 3 animals for the amphetamine/saline injection experiments (asterisks indicate significance at the $p < 0.01$ level; paired *t*-test).

in k_2 and $k_{2\alpha}$. An association between regional DA signalling dynamics and the behavioural effect of the drug is, therefore, clearly evident.

Fig. 6a shows the behavioural analysis of a representative animal throughout the amphetamine and saline vehicle PET scans. The animal exhibited similar behavioural profiles during the first 20 min of each scan, prior to drug or vehicle administration (Fig. 6a). Following amphetamine administration (Fig. 6b), the rat showed a marked increase in repetitive locomotive stereotyped behaviour. It repeatedly adopted a unique "perched" position and alternately sniffed the base and top of the scanner (Fig. 6c). In contrast, following vehicle administration the rat maintained moderate to low levels of sniffing behaviour in a non-perched position and other non-stereotypical behaviours, such as sleeping and grooming. The observed changes in behaviour following amphetamine administration are consistent with previous studies (Lindquist et al., 1977; Schiorring, 1979) and can be attributed to activation of the thalamo-striatal pathway via sudden release of endogenous dopamine. Together with the results shown in the previous section and Figs. 4 and 5, the current study provides evidence of in vivo changes in D2R occupancy and simultaneous changes in behaviour due to amphetamine administration to awake, freely moving rats.

5. Discussion

We have developed an open-field PET system that addresses three fundamental limitations of small animal neuroimaging studies: (i) it overcomes the confounding effects of common anaesthetic drugs on neurophysiological parameters such as cerebral blood flow, neurotransmitter release and receptor occupancy (Martin et al., 2006; Ohba et al., 2009); (ii) it enables the study of neurochemical responses to sensory stimuli that require the conscious attention of the animal (Tsukuda et al., 2002); and (iii) it enables the concurrent study of regional neurotransmitter-receptor function and behavioural responses to drugs and other environmental stimuli in conscious, unrestrained animals. All of these advantages can be exploited in longitudinal study designs because the technique allows repeat experiments on the same animal.

Using this technique, we demonstrated that it is possible to reproducibly detect and quantify, in awake and freely moving animals, a pharmacologically induced displacement of [^{11}C]raclopride from D2 receptors by administering unlabelled raclopride, with reliable estimates of the magnitude and time of displacement onset. We also demonstrated the concurrent measurement of changes in receptor-ligand binding and behaviour; specifically, we measured changes in D2 receptor binding, locomotion and stereotypy associated with stimulation of dopamine release following the administration of amphetamine to awake, freely moving rats. Importantly, the technology we have developed allows us to reproducibly associate a measurable functional response in the brain to a diverse range of locomotor activity responses – from reduced (e.g. cold raclopride) to extreme increase (e.g. amphetamine) in locomotor activity.

Since we are considering a non-steady state regime in which the injection of the drug affects the physiology and the kinetic parameters (especially $k_{2\alpha}$) in a time dependent manner, conventional models such as the SRTM or MRTM are no longer valid (Alpert et al., 2003). We demonstrated quantifiable displacement in the time-varying receptor binding using the lp-ntPET model (Normandin et al., 2012) in conjunction with statistical confidence modelling using the ABC method (Marin et al., 2012). We believe this is the first study to report the relative magnitude of ligand displacement following drug challenge for awake rodents.

To our knowledge, this is also the first report of a complete motion compensation-based solution for freely moving rats during PET imaging. A related approach for single photon emission computed tomography (SPECT) of awake mice was reported by Baba et al. (2013), however the system was limited to tube-bound animals. Several alternative

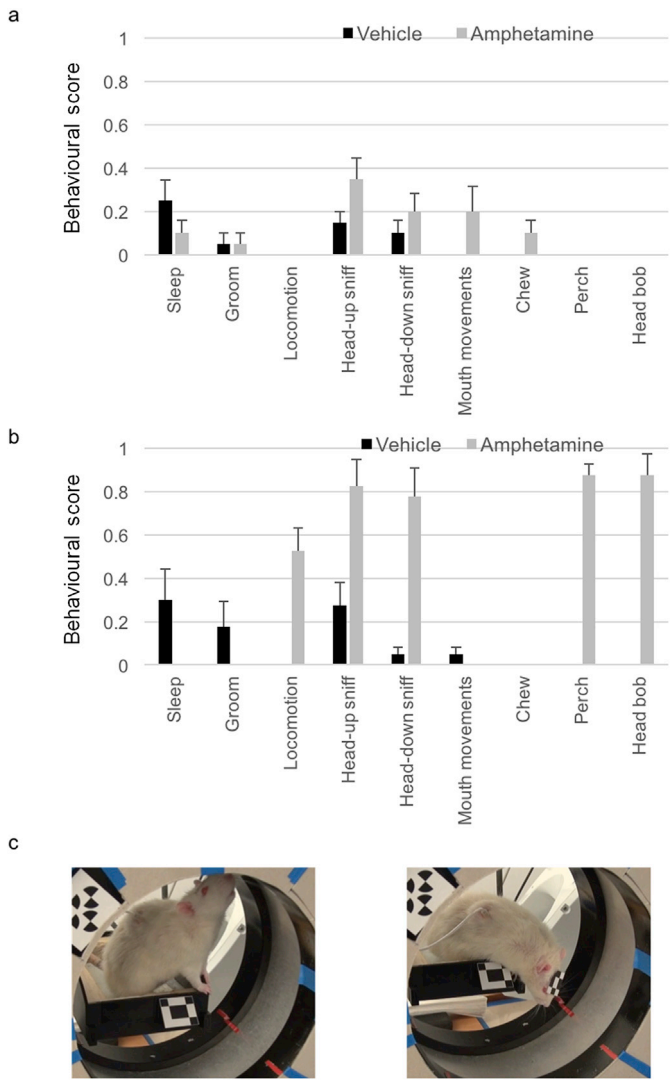

Fig. 6. Analysis of behaviours during open-field PET studies.
Analysis of stereotypical and non-stereotypical behaviours exhibited throughout the open-field PET scans in Figs. 4 and 5 by a representative rat: (a) behavioural score for a range of different behaviours (Table 1) during the 20 min prior to drug or saline vehicle administration; (b) behavioural score for a range of different behaviours during the 40 min following drug or saline vehicle administration. Scores are based on the proportion of time spent exhibiting a given behaviour during each 1 min interval (Kelley, 1998), averaged over the full observation period. Error bars represent standard error of the mean; (c) still frames of the video taken during the open-field PET study demonstrating stereotypical head-up (left) and head-down (right) sniffing in a perched position.

approaches for tracking animal head motion have been reported which could be substituted for our tracking method, providing potential advantages. For example, marker-free tracking based on native features (Kyme et al., 2014) or structured light (Miranda et al., 2017) avoids the problem of head-marker decoupling, and tracking of radioactive fiducials glued to the head avoids the need for additional tracking hardware (Miranda et al., 2018) – though the latter approach is only useful when the animal is inside the FoV. A further motion tracking improvement relates to lighting: currently, the animals are pre-acclimatised to visible lighting needed for motion tracking. Although this lighting is diffuse and outside the animal's direct line-of-sight, and we have not observed any evidence that it perturbs them, the ability to perform infra-red based tracking (Baba et al., 2013) in darkened conditions is preferable for nocturnal subjects and would likely facilitate a greater range of experiments.

The system described in this report is based on a commercially available small animal PET system without modification, other than replacement of the animal support pallet with a robotically controlled enclosure and a mechanism to synchronise motion tracking and PET data. Thus, the open-field PET system could, in principle, be deployed where there is a suitable commercial small animal PET scanner. However, it has some limitations that may affect performance of the PET study. For example, the robot is programmed to translate the animal enclosure relatively slowly (max speed 1.6 cm s^{-1}) with smooth acceleration and deceleration to avoid startling the animal. For a typical scan, this may lead to the animal spending on average $< 5\%$ of the time outside the active FoV during a scan, which has a negligible effect on the acquired dynamic data. However, when the animal is more active, such as with an amphetamine challenge, on average it may spend a larger portion of the PET study (approximately 40%) with its brain outside the active FoV of the scanner, resulting in significant loss of counts. Similarly, the animal may move to blind spots (where tracking line-of-sight is obstructed), causing temporary loss of data. While we can account for temporary loss of data within the reconstruction software, it negatively impacts signal-to-noise ratio, thus reducing the statistical reliability of parameter estimation.

It is clear that several motion-related factors can potentially impact the accuracy and/or precision of reconstructed images and estimated regional end-point parameters in our approach:

(i) Potential resolution loss due to insufficient motion sampling and/or off-centre animal locations;
(ii) Potential increased noise due to periods of unknown motion (blind spots) and/or loss of counts when the animal is outside the FoV.

In general, resolution loss is a minor effect (Angelis et al., 2018). The use of high frame-rate tracking (30 Hz) mitigates motion sampling-related error (Angelis et al., 2018; Kyme et al., 2011) and lateral movement of the robotic enclosure allows us to minimise the time the animal is located off-centre transaxially. We used a spatially invariant kernel for resolution modelling which is optimal at the centre (Angelis et al., 2015). A spatially variant kernel (Bickell et al., 2016) may provide further improvement but we have not investigated this. Regarding noise, the inter-voxel variance of a uniform ROI certainly increases as a function of the duration of the tracking gap or loss of counts, however we have also observed that bias remains $<0.5\%$ even when the decrease in counts is $>90\%$ (unpublished data). We are currently seeking to address several of the motion-related factors impacting performance by developing a modified open-field PET system that translates a lightweight PET detector ring, rather than the enclosure, in response to animal movement (Kyme et al., 2017), thus enabling rapid compensatory movements without startling the animal and without loss of data.

We believe studies of reward-driven learning and plasticity will be an important area of application for the open-field PET technique. The capacity to measure endogenous neurotransmitter release at the whole-brain level with accurate estimation of the location and timing of activation onset, while simultaneously recording behavioural responses, is essential if we are to gain new insights into the role of specific brain circuits and neurotransmitters in mediating reward prediction and behavioural adaptation. The design of the animal enclosure as an operant conditioning chamber facilitates such studies where, instead of drug administration, the animal learns a contingency between a visual or auditory stimulus and a reward. Other important applications include drug addiction studies and investigations of pathological conditions, such as post-traumatic stress disorder, that impede the ability of an animal to respond appropriately to external stimuli and adapt to a changing environment.

Author contributions

SRM and RRF conceived the open-field PET method. AZK, JE, VZ, GH, BWB and SRM developed the observation chamber; AZK, GIA, RRF and

VZ developed the motion tracking methodology; JE, AZK and VZ developed the robot control algorithm; GIA, RRF, VZ, WJR, AZK, MA and SRM developed the motion correction and image reconstruction methodology; G Pascali and G Perkins produced and optimised the radiotracer; KJC and GH performed the surgery; GIA, GH, AZK and KP trained the animals; GIA, AZK, GH, JE, KP and AP performed the PET studies; GIA, SRM, GH and AZK performed data analysis; AZK, GIA and SRM prepared the manuscript; all authors read and edited the manuscript.

Declaration of interests

None.

Acknowledgements

The authors gratefully acknowledge the following people for their advice and input on various aspects of this work: Richard Banati, Jonathon Arnold, Marie-Claude Grégoire, Arkadiusz Sitek, Marc Normandin and Nathaniel Alpert. This work was supported by the Australian Research Council (project grants DP0988166, DP120103813 and DP160105070) and the Australian Institute of Nuclear Science and Engineering (project grant ALNGRA15022). All work was conducted at the Sydney-ANSTO node of the Australian National Imaging Facility (www.anif.org.au) which is supported by the Commonwealth Government of Australia, the NSW Government, the University of Sydney and the Australian Nuclear Science and Technology Organisation (ANSTO). For part of this work, Andre Kyme was supported by a Cassen Postdoctoral Fellowship, Education and Research Foundation, Society Nuclear Medicine and Molecular Imaging, USA.

References

Alpert, M., et al., 2003. A novel method for noninvasive detection of neuromodulatory changes in specific neurotransmitter systems. Neuroimage 19 (3), 1049–1060.
Angelis, G.I., Bickell, M., Kyme, A., Ryder, W., Zhou, L., Nuyts, J., Meikle, S., Fulton, R., 2013. Calculated attenuation correction for awake small animal brain PET studies. In: Proc. 2013 IEEE Nucl. Sci. Symp. Med. Imaging Conf. https://doi.org/10.1109/NSSMIC.2013.6829263.
Angelis, G., et al., 2015. Full field spatially-variant image-based resolution modeling reconstruction for the HRRT. Phys. Med. 31 (2), 137–145.
Angelis, G., et al., 2018. Image-based modelling of residual blurring in motion corrected small animal PET imaging using motion dependent point spread functions. Biomed. Phys. Eng. Express 4, 035032.
Angelis, G.I., Kyme, A.Z., Ryder, W.J., Fulton, R.R., Meikle, S.R., 2014. Attenuation correction for freely moving small animal brain PET studies based on a virtual scanner geometry. Phys. Med. Biol. 59, 5651–5666.
Baba, J., et al., 2013. Molecular imaging of conscious, unrestrained mice with AwakeSPECT. J. Nucl. Med. 54 (6), 969–976.
Belle, A.M., Owesson-White, C., Herr, N.R., Carelli, R.M., Wightman, R.M., 2013. Controlled iontophoresis coupled with fast-scan cyclic voltammetry/electrophysiology in awake, freely moving animals. ACS Chem. Neurosci. 4, 761–771.
Bickell, M., et al., 2016. Spatially variant resolution modelling for iterative list-mode PET reconstruction. IEEE Trans. Med. Imag. 35 (7), 1707–1718.
Chatziioannou, A.F., 2002. Molecular imaging of small animals with dedicated PET tomographs. Eur. J. Nucl. Med. 29, 98–114.
Chen, J.L., Andermann, M.L., Keck, T., Xu, N.-L., Ziv, Y., 2013. Imaging neuronal populations in behaving rodents: paradigms for studying neural circuits underlying behavior in the mammalian cortex. J. Neurosci. 33, 17631–17640.
Cherry, S.R., 2011. Functional whole-brain imaging in behaving rodents. Nat. Methods 8 (4), 301–303.
Helmchen, F., Fee, M.S., Tank, D.W., Denk, W., Hill, M., 2001. A miniature head-mounted neurotechnique two-photon microscope : high-resolution brain imaging in freely moving animals. Neuron 31, 903–912.
Hillegaart, V., Ahlenius, S., 1987. Effects of raclopride on exploratory locomotor activity, treadmill locomotion, conditioned avoidance behaviour and catalepsy in rats: behavioural profile comparisons between raclopride, haloperidol and preclamol. Pharmacol. Toxicol. 60 (5), 350–354.
Hume, S.P., et al., 1995. Effect of L-dopa and 6-hydroxydopamine lesioning on [11C] raclopride binding in rat striatum, quantified using PET. Synapse 21, 45–53.
Hume, S.P., Gunn, R.N., Jones, T., 1998. Pharmacological constraints associated with positron emission tomographic scanning of small laboratory animals. Eur. J. Nucl. Med. 25, 173–176.
Ichise, M., et al., 2003. Linearized reference tissue parametric imaging methods: application to [11C]DASB positron emission tomography studies of the serotonin transporter in human brain. J. Cerebr. Blood Flow Metabol. 23, 1096–1112.
Kelley, A.E., 1998. In: Crawley, J.N., et al. (Eds.), Current Protocols in Neuroscience. John Wiley & Sons, pp. 8.8.1–8.8.13.
Kyme, A.Z., Zhou, V.W., Meikle, S.R., Fulton, R.R., 2008. Real-time 3D motion tracking for small animal brain PET. Phys. Med. Biol. 53, 2651–2666.
Kyme, A.Z., Zhou, V.W., Meikle, S.R., Baldock, C., Fulton, R.R., 2011. Optimised motion tracking for positron emission tomography studies of brain function in awake rats. PloS One 6, e21727. https://doi.org/10.1371/journal.pone.0021727.
Kyme, A., Meikle, S., Baldock, C., Fulton, R., 2012. Tracking and characterizing the head motion of unanaesthetized rats in positron emission tomography. J. R. Soc. Interface 9, 3094–3107.
Kyme, A., et al., 2014. Markerless motion tracking of awake animals in positron emission tomography. IEEE Trans. Med. Imag. 33 (11), 2180–2190.
Kyme, A., et al., 2017. Open-field mouse brain PET: design optimisation and detector characterisation. Phys. Med. Biol. 62, 6207.
Lindquist, M.P., Gotestam, K.G., 1977. Open-field behavior after intravenous amphetamine analogues in rats. Psychopharmacology (Berlin) 55, 129–133.
Marin, J.M., Pudlo, P., Robert, C.P., Ryder, R.J., 2012. Approximate Bayesian computational methods. Stat. Comput. 22, 1167–1180.
Martin, C., Martindale, J., Berwick, J., Mayhew, J., 2006. Investigating neural-hemodynamic coupling and the hemodynamic response function in the awake rat. Neuroimage 32, 33–48.
Miranda, A., et al., 2017. Markerless rat head motion tracking using structured light for brain PET imaging of unrestrained awake small animals. Phys. Med. Biol. 62 (5), 1744–1758.
Miranda, A., et al., 2018. Fast and accurate rat head motion tracking with point sources for awake brain PET. IEEE Trans. Med. Imag. 36 (7), 1573–1582.
Mizuma, H., Shukuri, M., Hayashi, T., Watanabe, Y., Onoe, H., 2010. Establishment of in vivo brain imaging method in conscious mice. J. Nucl. Med. 51, 1068–1075.
Nakao, Y., et al., 2001. Effects of anesthesia on functional activation of cerebral blood flow and metabolism. Proc. Natl. Acad. Sci. Unit. States Am. 98, 7593–7598.
Normandin, M.D., Schiffer, W.K., Morris, E.D., 2012. A linear model for estimation of neurotransmitter response profiles from dynamic PET data. Neuroimage 59, 2689–2699.
Ohba, H., Harada, N., Nishiyama, S., Kakiuchi, T., Tsukada, H., 2009. Ketamine/xylazine anesthesia alters [11C]MNPA binding to dopamine D2 receptors and response to methamphetamine challenge in monkey brain. Synapse 63, 534–537.
Patel, V.D., Lee, D.E., Alexoff, D.L., Dewey, S.L., Schiffer, W.K., 2008. Imaging dopamine release with positron emission tomography (PET) and 11C-raclopride in freely moving animals. Neuroimage 41, 1051–1066.
Perkins, G., Sheth, R., Greguric, I., Pascali, G., 2014. Optimisation of [11C]Raclopride production using a Synthra GPextent system. Curr. Rad. 7, 100–106.
Rahmim, A., et al., 2008. Accurate event-driven motion compensation in high-resolution PET incorporating scattered and random events. IEEE Trans. Med. Imag. 27, 1018–1033.
Schiorring, E., 1979. An open field study of stereotyped locomotor activity in amphetamine-treated rats. Psychopharmacology (Berlin) 66, 281–287.
Schulz, S., et al., 2011. Simultaneous assessment of rodent behavior and neurochemistry using a miniature positron emission tomograph. Nat. Methods 8, 347–352.
Tai, Y.C., et al., 2005. Performance evaluation of the microPET focus: a third-generation microPET scanner dedicated to animal imaging. J. Nucl. Med. 46, 455–463.
Tantawy, M., et al., 2011. Impact of isoflurane anesthesia on D2 receptor occupancy by [18F]fallypride measured by MicroPET with a modified logan plot. Synapse 65 (11), 1173–1180.
Thanos, P.K., et al., 2013. Mapping brain metabolic connectivity in awake rats with μPET and optogenetic stimulation. J. Neurosci. 33, 6343–6349.
Tsukada, H., Miyasato, K., Kakiuchi, T., Nishiyama, S., Harada, N., Domino, E.F., 2002. Comparative effects of methamphetamine and nicotine on the striatal [11C] raclopride binding in unanesthetized monkeys. Synapse 45, 207–212.
Vaska, P., 2004. RatCAP: miniaturized head-mounted PET for conscious rodent brain imaging. IEEE Trans. Nucl. Sci. 51, 2718–2722.
Vyazovskiy, V.V., et al., 2011. Local sleep in awake rats. Nature 472, 443–447.
Zhou, V.W., Kyme, A.Z., Meikle, S.R., Fulton, R.R., 2008. An event driven motion correction method for neurological PET studies of awake laboratory animals. Mol. Imag. Biol. 10, 315–324.
Zhou, V.W, et al., 2013. A motion adaptive animal chamber for PET imaging of freely moving animals. IEEE Trans. Nucl. Sci. 60, 3423–3431.